Bull. Mater. Sci., Vol. 39, No. 5, September 2016, pp. 1285–1294. © Indian Academy of Sciences.
DOI 10.1007/s12034-016-1259-y

# Structure and properties of silver-doped calcium phosphate nanopowders

**RAVINDER PAL SINGH* and UMA BATRA**
Department of Materials and Metallurgical Engineering, PEC University of Technology, Chandigarh 160012, India

MS received 20 October 2015; accepted 8 February 2016

**Abstract.** **Stable and antimicrobial silver-doped calcium phosphate nanopowders were synthesized using sol–gel route by setting the atomic ratio of Ag/(Ag + Ca) at 3% and (Ca + Ag)/P at 1.67. Prior to synthesis of nanopowders, influence of time of hydrolyzation on pH and density of precursors were comprehensively studied. Hydrolyzation time was found to have profound influence on pH of constituent precursors. Sufficient hydrolysis resulted in early maturation of sol. Scanning electron microscopy (SEM) showed the heterogeneous and agglomerated state of particles with average size of 3.9 ± 1.9 μm. Energy dispersive X-ray spectroscopy (EDX) presented uniform distribution of O, Ag, Ca and P elements in nanopowder. Fourier transform infrared spectroscopy (FTIR) confirmed the formation of apatitic structure, whereas X-ray diffraction (XRD) revealed the multiphase constitution of nanopowders primarily composed of β-TCP, Ag and other hybrid phases. Crystallite size and lattice parameters of β-TCP and Ag phases were increased with the rise in calcination temperature. Thermogravimetric analysis (TGA) showed three regions of weight change and indicated the high thermal stability of nanopowders. Disk diffusion method was used to test the antimicrobial resistance of nanopowders against *Escherichia coli* and *Staphylococcus aureus* bacterial strains. All nanopowders exhibited antimicrobial resistance against both *E. coli* and *S. aureus* bacteria.**

**Keywords.** **Sol–gel processes; calcination; electron microscopy; antimicrobial.**

## 1. Introduction

Success and long-term survival of orthopedic implants in human body depends on the prevention of bacterial infection which is usually encountered following the implant placement [1]. Infection is one of the devastating reasons which severely reduces the lifespan of the implants and increases their failure rates [2]. One simple and accepted strategy to treat and prevent infections associated with orthopedic implants is to deliver antibiotics in a controlled manner at the site of implantation [3–5]. Among the antibiotics, ionic heavy metals, such as $Ag^{+}$, $Zn^{2+}$ and $Cu^{2+}$ are efficient, stable and can be easily carried by calcium phosphate (CP)-based powders doped through ionic substitution or co-precipitation methods.

Ag shows a broad spectrum of antibacterial activity and possesses many advantages, such as excellent biocompatibility, satisfactory stability [6,7] and exhibits low toxicity towards mammalian cells [8]. Ag particles bind to the bacterial cell wall and cell membrane and inhibit their respiration process [9,10]. All common bacterial strains involved in implant-associated infections can be eliminated by Ag [2]. Influence of Ag concentration on physico-chemical and antimicrobial resistance of hydroxyapatite (HAP) nanopowders has been discussed by many workers [11–15]. Low concentrations of Ag lack the toxicity on the mammalian cells [16–18], but its high concentration could have toxic effects [1].

Ion exchange method is widely used for doping of Ag into HAP nanopowders. The limitation of this method is that the antimicrobial agent accumulates onto the surface and quickly depletes without long-term antimicrobial effect [12]. But, through sol–gel route, the substituted ions directly insert into the lattice structure of matrix elements [2,16] and produce stable compounds [17,19].

In this paper, sol–gel route was employed to synthesize Ag-doped calcium phosphate (Ag–CP) nanopowders. Ag concentration of 3 wt% has been suggested as an optimum dose with highest antimicrobial resistance along with least cytotoxic properties and therefore, was selected for the present investigation. Besides the detailed examination of physico-chemical properties of Ag–CP nanopowders, influence of time of hydrolyzation on pH and density of constituent precursors were also examined. Disk diffusion method was used to examine the antimicrobial resistance of synthetic nanopowders against microbiological assays of Gram negative *Escherichia coli* and Gram positive *Staphylococcus aureus* bacteria.

## 2. Materials and methods

Calcium nitrate tetrahydrate (CNT, Merck, 98%), triethyl phosphite (TEP, Spectrochem, 98%) and silver nitrate ($AgNO_3$, Merck, 99.9%) were used as Ca, P and Ag ion sources, respectively. Double-distilled water (DDW) and ethanol (Merck, 99.9%) were used as solvents. Ammonium hydroxide ($NH_4OH$, Merck, 25%) was used to improve the gelation. Synthesis procedure is detailed in figure 1.

*Author for correspondence (er.ravinderpalsingh@gmail.com)

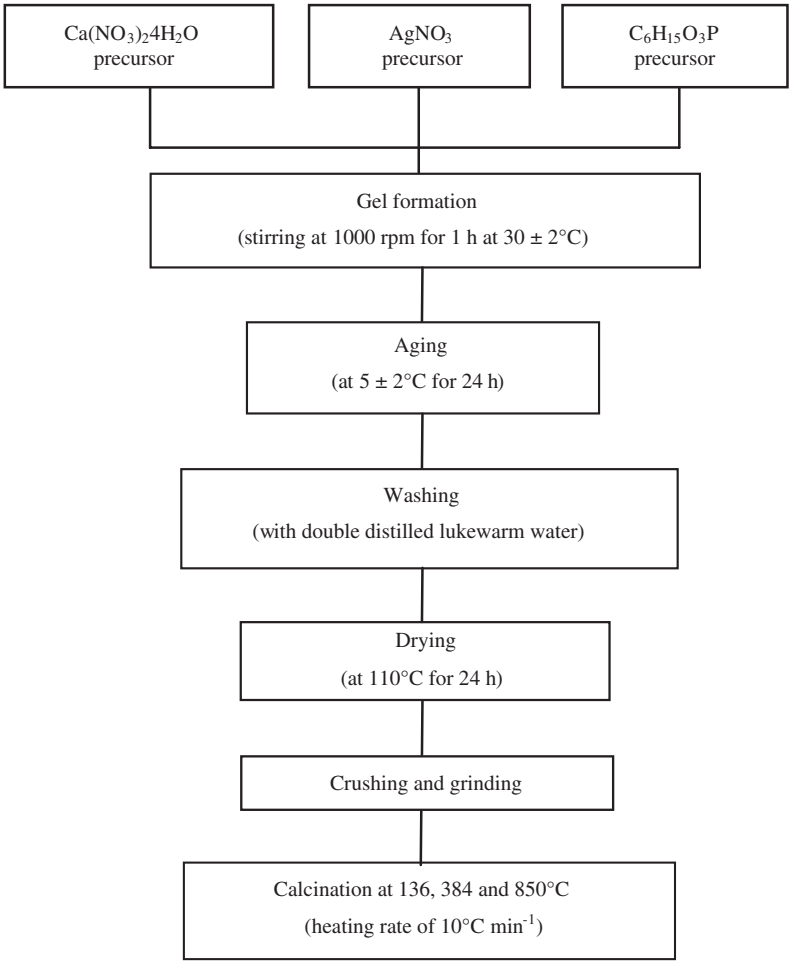


**Figure 1.** Synthesis procedure.

### 2.1 *Sol characterization*

Digital pH meter (MAX, India) and digital weighing-cum-density meter (Denver, SI-234) were used to measure the pH and density of solutions, respectively.

### 2.2 *Powder characterization*

Particle morphology was examined using scanning electron microscopy (SEM, JEOL), operated at 15 kV. Elemental composition of nanopowder was examined using colour mapping technique of energy dispersive spectroscopy (EDX).

Fourier-transform infrared spectra (FTIR, Perkin Elmer) were recorded in the range of 400–4000 $cm^{-1}$ using KBr pellets (1% wt/wt) with spectral resolution of 2 $cm^{-1}$ and taking 32 scans for each sample.

X-ray diffraction (XRD, Philips X'Pert 1710) analysis was performed using CuK$\alpha$ radiation ($\lambda = 1.54$ Å, $2\theta = 10$–$80°$, step size 0.017°, time per step 20.03 s and scan speed 0.005° $s^{-1}$). Relative amount of detected phases were estimated on the basis of the peak intensity variation by means of external standard method. Lattice parameters for $\beta$-TCP and Ag phases were calculated using equations (1) and (2), respectively:

$$\frac{1}{d^2} = \frac{4}{3}\left\{\frac{h^2 + hk + k^2}{a^2}\right\} + \frac{l^2}{c^2}, \tag{1}$$

$$\frac{1}{d^2} = \frac{h^2 + k^2 + l^2}{a^2}, \tag{2}$$

where $d$ is the distance between adjacent planes in the set of Miller indices ($hkl$). The JCPDS file nos. 01-070-0364 for $\beta$-TCP, 01-071-4613 for Ag (cubic, $a = 4.086$ nm), 01-084-1261 for silver oxide, 01-082-0807 for calcium phosphide, 00-054-1098 for silver calcium phosphate and 01-084-0511 for trisilver phosphate (cubic, $a = 6.011$ nm) were used.

Crystallite size ($X_S$) was calculated using Scherrer's formula (equation 3):

$$X_S = \frac{0.9\lambda}{\beta \cos\theta}, \tag{3}$$

where $X_S$ is in nanometer, $\lambda$ the wave length of X-ray beam, $\beta$ the broadening of diffraction line at half of its maximum intensity in radians and $\theta$ the Bragg's diffraction angle (°).

The silicon standard was used to measure the instrument broadening to correct the value of $\beta$.

Thermal behaviour of nanopowder was investigated using thermogravimetry (TG) (Perkin Elmer STA 6000) analyzer with an accuracy of $\pm 0.1$ μg in weight measurement and $\pm 0.5$°C in temperature measurement. Test was performed in air environment under the conditions: heating rate 10°C $min^{-1}$, peak temperature 1000°C and air flow 20 ml $min^{-1}$.

Antimicrobial resistance of nanopowders was tested against *E. coli* and *S. aureus* bacteria using disk diffusion method. The inoculums of microorganisms were prepared from fresh overnight broth cultures incubated at 37°C. Agar was poured into petri dishes to form thick layers and dense inoculums of the tested microorganisms were added to them. Petri plates were left for 10 min to dry in air. Nanopowders were put into the wells on the agar surface and incubated for 24 h at 37°C. Diameter of inhibition zones (mm) were taken as the measurement of antimicrobial resistance.

## 3. Results and discussion

### 3.1 *Hydrolysis of precursors*

Precursors of CNT, TEP and $AgNO_3$ were hydrolysed at $30 \pm 2$°C for six days and their pH and density are shown in figure 2. The pH of CNT precursor was increased from 4.45 to 5.56 during 96 h of hydrolysis, revealing its denitrification. The pH of TEP and $AgNO_3$ precursors was decreased up to 120 h as shown in figure 2b and c, which indicated the continuous release of protons (liberation of $H^+$) in them. Density of CNT and TEP precursors were remained unchanged, whereas density of $AgNO_3$ precursor decreased minutely as shown in figure 2d–f, respectively. Optically, CNT and TEP precursors were remained transparent, whereas $AgNO_3$ precursor was remained carbon black in colour throughout hydrolysis.

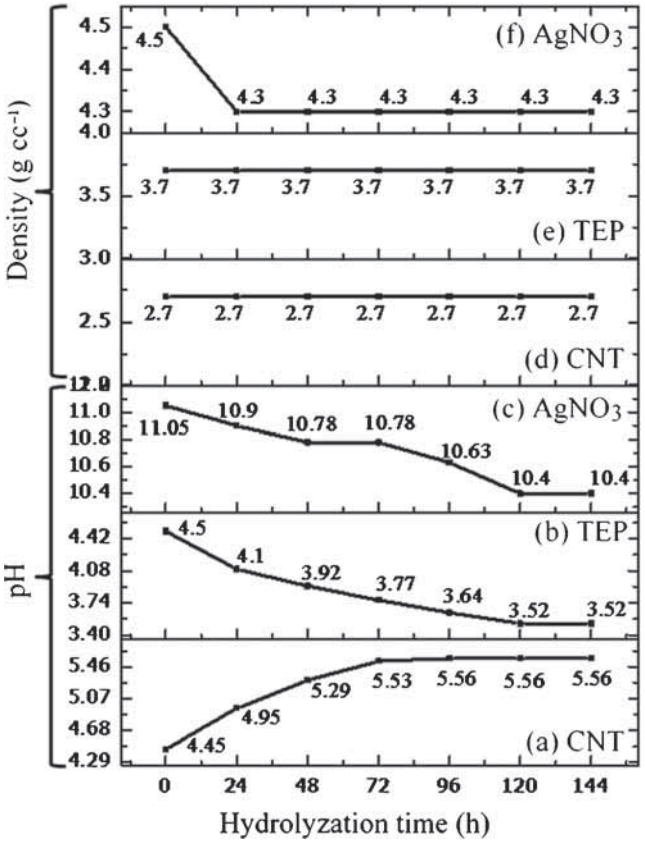


**Figure 2.** Influence of hydrolyzation time on pH: (**a**) CNT, (**b**) TEP, (**c**) $AgNO_3$ and density, (**d**) CNT, (**e**) TEP and (**f**) $AgNO_3$ precursors.

### 3.2 *Preparation of Ag–CP sol*

Matured CNT, TEP and $AgNO_3$ precursors were mixed together and formed Ag–CP sol. Incorporation of Ag ions into apatitic solution is based on equation (4) as suggested by Lim *et al* [20].

$$(10-x)Ca^{2+}(aq) + xAg^{+}(aq) + 6PO_4^{3-}(aq) + (2-x)OH^{-}(aq) \rightarrow Ca_{10-x}Ag_x(PO_4)_6(OH)_{2-x}(aq). \quad (4)$$

Milky white solution was developed upon the addition of $AgNO_3$ precursor into CNT precursor. Addition of TEP precursor transformed the resultant Ag–CP sol through various colour changes i.e., turned into light orange to red colour and finally to black colour during continuous stirring. No gelation was observed throughout the stirring. To cause precipitation, $NH_4OH$ was added into Ag–CP sol till its pH increased to 10. Optically, black coloured Ag–CP sol turned into light grey colour along with the development of gelation. The pH and density of Ag–CP sol were remained stable at 10 and 3.1 g $cc^{-1}$, respectively, throughout the ageing time period of 24 h.

Ammonia reacts readily with Ag ions in the basic conditions and form diamine silver (I) ion and reduces the incorporation of Ag ions into the apatite structure as suggested by various authors [20–22].

### 3.3 *Morphological and elemental properties of nanopowder*

Owing to its maximum crystallinity, Ag–CP nanopowder calcined at 850°C (Ag–CP-850) were characterized for particle shape, size and distribution. SEM micrographs of Ag–CP-850 nanopowder are shown in figure 3. Particles were aggregates of heterogeneous shapes and sizes. Spherical, elongated and small plate like particles were observed as shown in figure 3. Average particle size was $3.9 \pm 1.9$ μm, whereas average size of agglomerates was $4.4 \pm 2.1$ μm. Large surface area and high surface energy were usually associated with the nanoparticles which cause the particles to agglomerate.

Coagulation of HAP/Ag particles has been reported by Diaz *et al* [14]. Iqbal *et al* [23] reported agglomerated spherical morphology of HAP/Ag nanoparticles with particle size range of 80–85 nm. Ciobanu *et al* [24] reported ellipsoidal

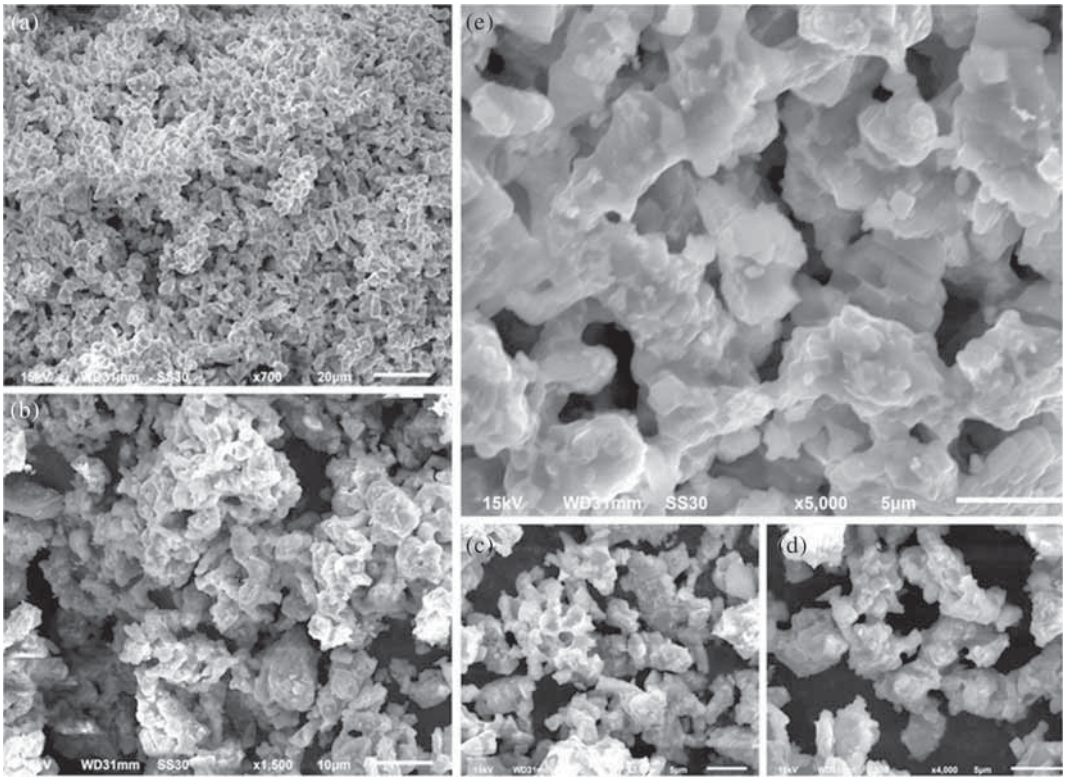


**Figure 3.** Particle morphology and distribution of Ag-CP–850 nanopowders shown at different magnifications.

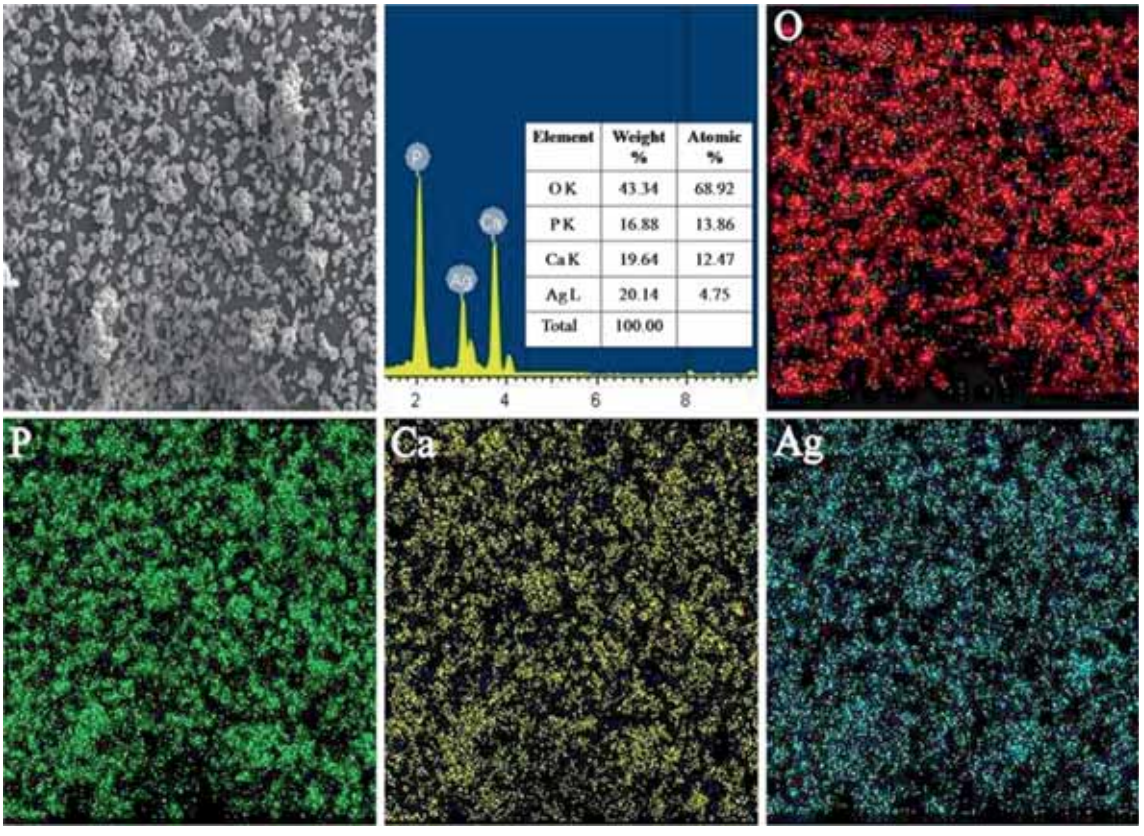


**Figure 4.** Elemental composition and distribution in Ag–CP-850 nanopowder.

morphology of HAP/Ag ($0.2 < x_{Ag} < 0.4$) particles. Size and shape of particles would influence their antimicrobial efficacy as reported by many workers [25–28]. Nanoparticles have large surface area and cause high percentage of interaction with bacterial cells than bigger particles as suggested by many workers [27–30]. According to Pal *et al* [28], truncated triangular nanoparticles showed bacterial inhibition with Ag content of 1 μg, whereas in case of spherical nanoparticles, total Ag content of 12.5 μg was needed. The rod-shaped particles needed 50–100 μg of Ag content.

Elemental composition and spread in Ag–CP-850 nanopowder is shown in figure 4. Uniform spread of O, Ca, P and Ag elements was noticed. The Ca/P molar ratio was 1.16 which inferred that some $Ca^{2+}$ ions in the apatite lattice were replaced or occupied by $Ag^{+}$ ions as suggested by Yang *et al* [31]. Ca/O ratio was 0.45 which was close to the standard value of 0.30 for HAP nanoparticles.

Ciobanu *et al* [12,24] and Iqbal *et al* [23] reported the presence of O, Ca, P and Ag elements in HAP/0.2 Ag-doped nanopowders. Feng *et al* [32] reported 1.19 and 1.46 Ca/P atomic ratio of coatings with and without Ag-treatment, respectively. They also reported the (Ca+Ag)/P molar ratio of 2.59 which was close to the similar ratio of 2.35 in the present study. Yang *et al* [31] reported Ca/P molar ratio of 1.529 of porous HAP/Ag nanocomposites. Bai *et al* [33] deposited functionally graded HAP coatings having 3% Ag content and detected Ca/P molar ratio of $2.33 \pm 0.01$.

### 3.4 *Ionic structure*

FTIR spectra of as-prepared and calcined Ag–CP nanopowders are shown in figure 5. Spectra confirmed the presence of apatitic peaks: structural $OH^{-}$ (630 $cm^{-1}$), $\nu_1PO_4^{3-}$ (962 $cm^{-1}$), $\nu_3PO_4^{3-}$ (1043 $cm^{-1}$) and $\nu_3HPO_4^{3-}$ (1131 $cm^{-1}$) ions in as-prepared and calcined Ag–CP nanopowders. Small peaks corresponding to $OH^{-}$ water (1629 $cm^{-1}$), P–OH (2462 $cm^{-1}$) and surface adsorbed water ions (3392 $cm^{-1}$) were also present in as-prepared and Ag–CP nanopowder calcined at 136°C (Ag–CP-136) as shown in figure 5a and b. On calcination at 384°C (Ag–CP-384) and 850°C (Ag–CP-850), peaks of $OH^{-}$ water and surface adsorbed water ions disappeared from the spectra as shown in figure 5c and d. $CO_3^{2-}$ peaks (1300–1600 $cm^{-1}$) appeared in the spectra of Ag–CP-384 and Ag–CP-850 nanopowders, which indicated the formation of carbonated apatitic structure in these nanopowders. Some unwanted peaks which might belong to the compounds, used while making the pallets, were also detected in spectra of Ag–CP-850 nanopowder (figure 5d) and were not considered. High concentration of $PO_4^{3-}$ ions suggested the formation of nonstoichiometric Ca/P molar ratio in Ag–CP nanopowders.

Presence of $\nu_1PO_4^{3-}$ ion (950–975 $cm^{-1}$) indicated the formation of $\beta$-TCP phase in Ag–CP nanopowders as suggested by Vijayalakshmi and Rajeswari [34]. Disappearance of $OH^{-}$ and surface adsorbed water ions have suggested the substitution of $Ag^{+}$ into $Ca^{2+}$ ions as reported by many workers [12,24,35,36].

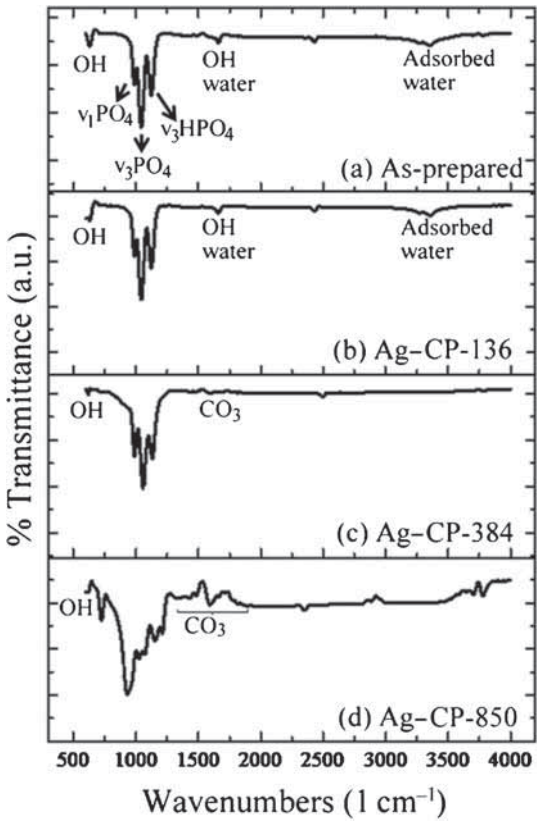


**Figure 5.** FTIR spectra of (**a**) as-prepared, (**b**) Ag–CP-136, (**c**) Ag–CP-384 and (**d**) Ag–CP-850 nanopowders.

### 3.5 *Phase constitution*

XRD patterns of as-prepared and calcined Ag–CP nanopowders are shown in figure 6. XRD patterns revealed the multiphase constitution of nanopowders composed of $\beta$-TCP, calcium phosphide ($Ca_5P_8$), Ag, silver oxide ($Ag_3O_4$) and other hybrid phases as shown in figure 6. Presence of pure and oxide phases of Ag indicated the successful doping of CaP crystals with Ag. Several reports have demonstrated the high reactivity of (1 1 1) Ag facets [37–39]. Only $\beta$-TCP and trisilver phosphate ($Ag_3PO_4$) phases were present in Ag–CP-850 nanopowder as shown in figure 6d. Development of trisilver phosphate phase suggested the chemical reaction of Ag with $PO_4^{3-}$ ions. Satisfactory match in terms of peak positions and peak intensities in as-prepared and calcined Ag–CP nanopowders was observed on comparing with the standard JCPDS files of constituent phases. Weight% of constituent phases is mentioned in table 1.

The isolated (2 2 0) and (2 1 4) reflections were used to calculate the crystallite size and lattice parameters of hexagonal $\beta$-TCP crystals, whereas (2 2 0) and (3 1 1) planes were used to calculate the crystallite size and lattice parameters of cubic Ag phase in Ag–CP nanopowders. Mean crystallite size and lattice parameters of $\beta$-TCP and Ag phases were increased with the rise in calcination temperature as mentioned in table 2. Lattice parameter of Ag crystal remained close to the standard value of 4.086 up to the calcination temperature of 136°C.

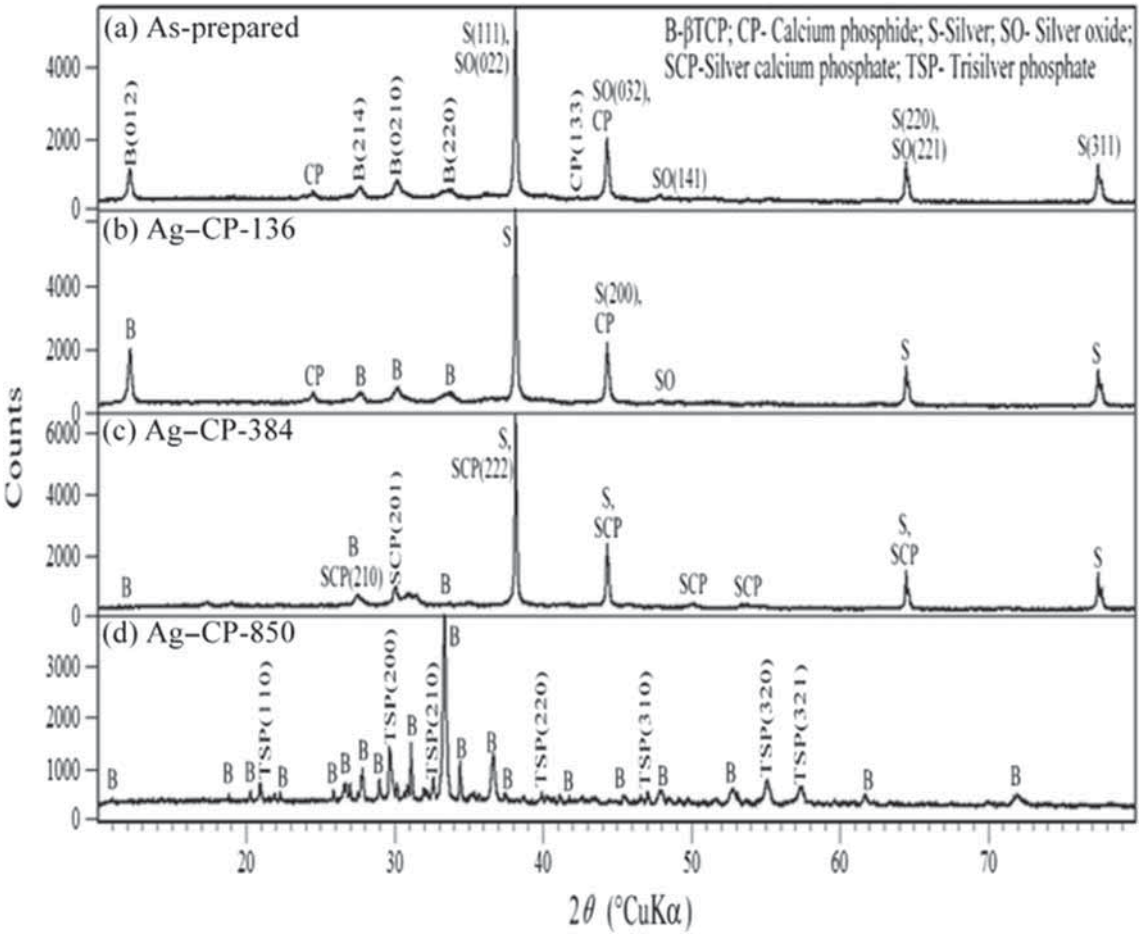


**Figure 6.** XRD patterns of (**a**) as-prepared, (**b**) Ag–CP-136, (**c**) Ag–CP-384 and (**d**) Ag–CP-850 nanopowders.

**Table 1.** Weight percentage of constituent phases in as-prepared and calcined Ag–CP nanopowders.

| Weight percentage | Nanopowders | | | |
|---|---|---|---|---|
| | As-prepared | Ag–CP-136 | Ag–CP-384 | Ag–CP-850 |
| $\beta$-TCP | 51 | 51 | 15 | 61 |
| CP | 9 | 11 | – | – |
| S | 33 | 35 | 54 | – |
| SO | 7 | 3 | – | – |
| SCP | – | – | 31 | – |
| TSP | – | – | – | 39 |

Rameshbabu *et al* [15] produced HAP/Ag nanopowders and calcined below 700°C and reported single-phase apatite having low Ag content (<1.63 wt%). However, $\beta$-TCP and Ag phosphate phases were developed, when heated above 700°C and metallic Ag was observed, when heated at 800°C. Yang *et al* [31] observed HAP and Ag phosphate phases in co-precipitated porous HAP/Ag nanocomposites. The advantages of Ag phosphate phase compared to other Ag compounds are its low solubility in aqueous solutions and its high antibacterial efficiency as reported by Buckley *et al* [40] and Yi *et al* [41]. Diaz *et al* [14] detected no phases other than HAP and Ag in the nanocomposite of HAP/Ag prepared by co-precipitation method. Singh *et al* [11] reported phase-pure apatite having Ag content up to 2 wt%. Iqbal *et al* [23] detected HAP, Ag and $\beta$-TCP phases in HAP/Ag nanopowders. Ciobanu *et al* [24] observed only HAP phase in HAP/Ag ($0.2 < x_{Ag} < 0.4$) nanopowders. A small peak of Ag phase among HAP peaks was detected in the co-precipitated composites of HAP/Ag nanopowders as reported by Iqbal *et al* [42]. Akhavan *et al* [43] observed monoclinic Ag and Ag phosphate phases in $\gamma$-irradiated HAP/Ag nanoparticles. Lim *et al* [20] reported thermal stability (up to 1150°C) of co-precipitated phase-pure HAP/Ag nanoparticles containing 0.2–1.1 wt% of Ag.

Castanon *et al* [44] synthesized Ag particles of 25 nm. Diaz *et al* [14] reported Ag particles of 65 nm. Sygnatowicz *et al* [45] detected (1 1 1) and (2 0 0) planes of Ag particles of ∼100 nm crystallite size. Ciobanu *et al* [12] synthesized HAP/0.2 Ag nanoparticles using co-precipitation method and reported particle size of ∼40 nm. Iqbal *et al* [42] reported crystallite size of Ag phase with a range of 18–33 nm. Average size of HAP/Ag nanoparticles was 79 ± 26 nm as reported by Mocanu *et al* [46]. Lattice parameters of HAP

**Table 2.** Mean crystallite size and lattice parameters of $\beta$-TCP and Ag phases in as-prepared and calcined Ag–CP nanopowders.

| | Nanopowders | | | |
|---|---|---|---|---|
| | As-prepared | Ag–CP-136 | Ag–CP-384 | Ag–CP-850 |
| *Mean crystallite size (nm)* | | | | |
| $\beta$-TCP | 22.3 ± 6.1 | 49 ± 9.7 | 53.4 ± 11 | 62.1 ± 13 |
| Ag | 65.2 ± 13 | 89.2 ± 5.1 | 96.8 ± 5 | – |
| *Lattice parameters* | | | | |
| $\beta$-TCP | | | | |
| $a$ (Å) | 10.572 | 10.599 | 10.658 | 10.740 |
| $c$ (Å) | 33.555 | 34.645 | 34.948 | 35.355 |
| $c/a$ | 3.17 | 3.26 | 3.27 | 3.29 |
| Ag | | | | |
| $a$ (Å) | 4.087 | 4.087 | 5.468 | – |

in calcined HAP/Ag nanocomposites were: $a = 9.38587 \pm 0.00267$ Å, $c = 6.85981 \pm 0.00398$ Å as revealed by Nath *et al* [36]. Lattice parameters of $a = b = 9.435$ Å, $c = 6.876$ Å for $x_{Ag} = 0.05$; $a = b = 9.443$ Å, $c = 6.875$ Å for $x_{Ag} = 0.2$; and $a = b = 9.445$ Å, $c = 6.877$ Å for $x_{Ag} = 0.3$ were reported by Ciobanu *et al* [44]. Ciobanu *et al* [24] revealed the lattice parameters of $a = b = 9.422$ Å and $c = 6.879$ Å with $x_{Ag} = 0.2$; $a = b = 9.423$ Å and $c = 6.878$ Å for $x_{Ag} = 0.3$ and $a = b = 9.427$ Å and $c = 6.877$ Å for $x_{Ag} = 0.4$, respectively.

### 3.6 *Thermal properties*

TG plot of as-prepared Ag–CP nanopowder is shown in figure 7. Three regions of weight change marked as I, II and III were observed and are shown in figure 7. Region I: 30–136°C (weight increased by 4.72%), region II: 136–384°C (weight loss of 7.6%) and region III: 384–850°C (weight increased by 3.8%). Weight loss from 136 to 384°C was attributed to the escape of volatile OH and surface adsorbed water molecules. Weight loss of ∼7.6% indicated the high thermal stability of synthetic nanopowder. Due to the incorporation of Ag in the lattice, thermal stability of CaP powders increased as suggested by Nath *et al* [36]. It was supported by FTIR (figure 5) and XRD (figure 6) analyses also which revealed intact molecular and phase constitutions up to calcination temperature of 384°C.

### 3.7 *Antimicrobial resistance*

As-prepared and calcined Ag–CP nanopowders exhibited antimicrobial resistance against both *E. coli* and *S. aureus* bacteria, as inhibition zone developed around them as shown in figures 8 and 9. Pure CP nanopowders (without Ag) calcined at 300, 500, 700 and 900°C were also tested against both *E. coli* and *S. aureus* bacteria, but did not show antimicrobial resistance as shown in figure 10a and b. Structural and physico-chemical properties of these calcined CP

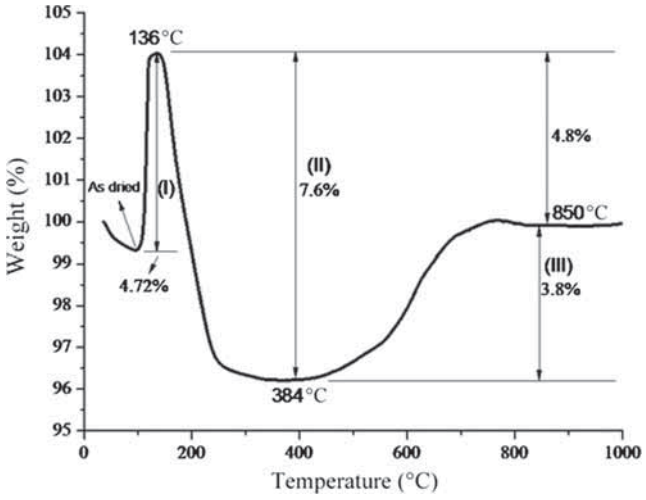


**Figure 7.** TG thermograph of as-prepared Ag–CP nanopowder.

nanopowders have been published elsewhere [47]. Average diameter of inhibition zones developed against *E. coli* and *S. aureus* bacteria are mentioned in table 3.

Calcined Ag–CP nanopowders exhibited superior antimicrobial resistance than as-prepared nanopowders as indicated by the diameter of inhibition zones mentioned in table 3. Ag–CP nanopowders exhibited superior resistance against *S. aureus* bacteria than *E. coli*.

Actual bactericide mechanism of Ag nanoparticles is not well known as reported by many authors [48,49]. Some researchers support the idea that Ag species release $Ag^+$ ions and interact with thiol groups in bacteria proteins, affect their DNA and inhibit bacterial replication [50].

Rameshbabu *et al* [15] observed complete inhibition of *S. aureus* bacteria after 24 h in co-precipitated HAP/Ag nanopowders containing 0.5, 1 and 1.5 wt% of Ag. Stanic *et al* [51] observed complete reduction of *S. aureus* bacteria after 4 h in co-precipitated nanodimensional HAP/Ag particles with 0.4 wt% of Ag. Singh *et al* [11] reported antibacterial effect against *E. coli* bacteria among co-precipitated

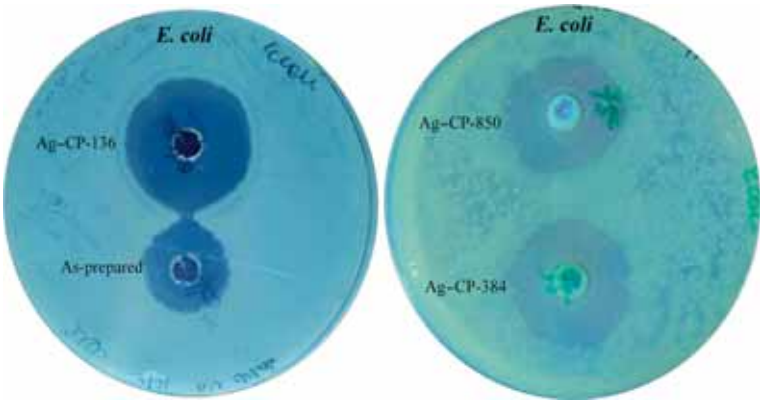


**Figure 8.** Inhibition zones developed around as-prepared and calcined Ag–CP nanopowders against *E. coli* bacteria.

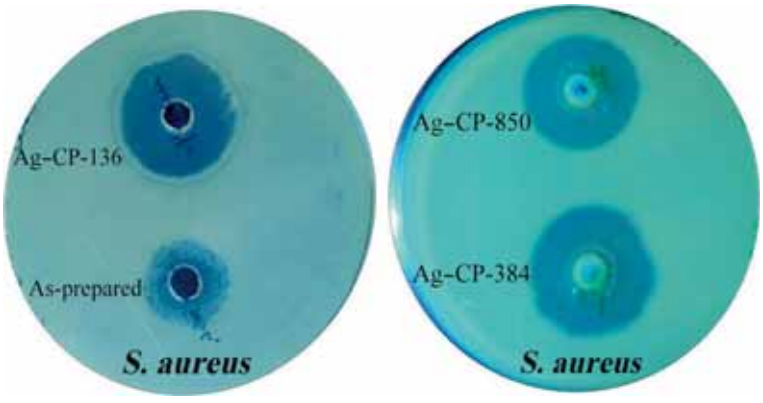


**Figure 9.** Inhibition zones developed around as-prepared and calcined Ag–CP nanopowders against *S. aureus* bacteria.

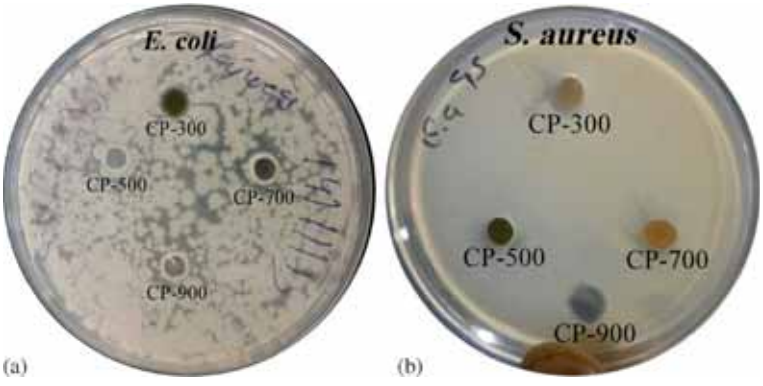


**Figure 10.** Petri dishes carrying calcined CP nanopowders tested against (**a**) *E. coli* and (**b**) *S. aureus* bacteria.

**Table 3.** Diameter of inhibition zones developed against *E. coli* and *S. aureus* bacteria.

| | Inhibition zone diameter (±1 mm) | | | | | | | |
|---|---|---|---|---|---|---|---|---|
| Nanopowders | As-prepared | Ag–CP-136 | Ag–CP-384 | Ag–CP-850 | CP-300 | CP-500 | CP-700 | CP-900 |
| *E. coli* | 15 | 22 | 50 | 48 | – | – | – | – |
| *S. aureus* | 41 | 56 | 60 | 56 | – | – | – | – |

HAP/Ag particles containing Ag content of 2, 3 and 5 wt%. However, HAP/Ag powders with Ag content greater than 3 wt% were cytotoxic towards mouse fibroblast cells. It has been suggested that Ag content between 0.5 and 3 wt% in co-precipitated HAP/Ag could achieve effective antibacterial effect [15,21,51]. A 3-log reduction of *S. aureus* population was observed in nanodimensional HAP/Ag particles containing 0.5, 0.9, 1 and 1.1 wt% of Ag as reported by Lim *et al* [52]. Substitution of 0.5 wt% of Ag into HAP was sufficient to retard and inhibit the bacterial growth. HAP/Ag powders exhibited complete inhibition of *E. coli* bacteria after 24 h as reported by Akhavan *et al* [43]. Several antibacterial studies demonstrated that HAP/Ag (both co-precipitated and ion exchanged) nanopowders exhibited excellent antibacterial activity, with a reduction of more than 99% against almost all known bacteria as reported by Lim *et al* [20].

Diaz *et al* [14] reported inhibition zone diameters of 18 ± 5 and 17 ± 0.5 mm developed around HAP/Ag nanopowders against *E. coli* and *S. aureus* bacteria, respectively. Mocanu *et al* [46] reported 10–15 mm and 11–16 mm inhibition zone diameters developed around HAP/Ag nanoparticles against *E. coli* and *S. aureus* bacteria, respectively. They also reported that *S. aureus* bacteria exhibited highest sensitivity against Ag nanoparticles, showing the largest zones of inhibition. Average diameter of inhibition zones were 4, 1 and 1 mm against *E. coli*, *S. aureus* and *Candida albicans* bacteria, respectively, exhibited by HAP/Ag nanopowders as revealed by Stanic *et al* [51]. Average inhibition zone diameters of HAP/0.3 Ag were 9, 6, 8 and 10 mm against *S. aureus*, *Bacillus subtilis*, *Pseudomonas aeruginosa* and *E. coli* bacteria, respectively, whereas HAP/1 Ag resulted in the inhibition zones of 5, 9, 8 and 10 mm, respectively. HAP/5 Ag showed inhibition diameters of 11, 9, 9 and 12 mm against *S. aureus*, *B. subtilis*, *P. aeruginosa* and *E. coli* bacteria, respectively, as reported by Iqbal *et al* [23].

## 4. Conclusion

Hydrolysis of constituent precursors must be completed before their mixing to form Ag–CP sol. Synthetic nanopowder was the agglomerated mixture of spherical, elongated and small plate-like particles of vivid sizes. EDX confirmed the uniform spread of all desirable elements. FTIR and XRD examinations confirmed the Ag-doped apatitic structure of synthesized nanopowders. Mean crystallite size and lattice parameters of primary phases were increased with the rise in calcination temperature. TG test indicated the high thermal stability of synthesized nanopowders and supported XRD and FTIR interpretations. All synthetic nanopowders were potent against selected bacterial strains. Nanopowders exhibited maximum antibacterial resistance against *S. aureus* bacteria.

## References


[1] Chen W, Liu Y, Courtney H S *et al* 2006 *Biomaterials* **27** 5512

[2] Miranda M, Fernández A and Díaz M 2010 *Int. J. Mater. Res.* **101** 122

[3] Hendriks J G E, Horn J R V, Mei H C V and Busscher H J 2004 *Biomater.* **25** 545

[4] Gerhart T N, Roux R D and Hanff P A 1993 *J. Orthopaed. Res.* **11** 250

[5] Leach W J and Wilson N I L 1992 *J. R. Col. Surg. Edinb.* **37** 265

[6] Zhao L, Chu P K and Zhang Y 2009 *J. Biomed. Mater. Res. Part B: Appl. Biomater.* **91** 470

[7] Babu R, Zhang J, Beckman E J *et al* 2006 *Biomaterials* **27** 4304

[8] Park E J, Lee S W and Bang I C 2011 *Nanoscale Res. Lett.* **6** 223

[9] Rai M, Yadav A and Gade A 2009 *Biotechnol. Adv.* **27** 76

[10] Feng Q L, Wu J and Chen G Q 2000 *J. Biomed. Mater. Res.* **52** 662

[11] Singh B, Dubey A K, Kumar S, Saha N, Basu B and Gupta R 2011 *Mater. Sci. Eng. C* **31** 1320

[12] Ciobanu C S, Massuyeau F, Constantin L V *et al* 2011 *Nanoscale Res. Lett.* **6** 613

[13] Kim J S, Kuk E, Yu K N and Kim J H 2007 *Nanomed. Nanotechnol. Biol. Med.* **3** 95

[14] Dıaz M, Barba F, Miranda M, Guitian F, Torrecillas R and Moya J S 2009 *J. Nanomater.* **2009** doi: 10.1155/2009/498505

[15] Rameshbabu N, Kumar S T S, Prabhakar T G, Sastry V S, Murty K V G K and Prasad R K 2007 *J. Biomed. Mater. Res.* **80A** 581

[16] Melaiye A and Youngs W J 2005 *Expert Opin.* **15** 125

[17] Mo A, Liao J and Xu W 2008 *Appl. Surf. Sci.* **255** 435

[18] Sondi I and Ba S S 2004 *J. Coll. Interf. Sci.* **275** 177

[19] Fielding G A, Roy M and Bandyopadhyay A 2012 *Acta Biomater.* **8** 3144

[20] Lim P N, Chang L and Thian E S 2015 *Nanomed.: Nanotechnol. Biol. Med.* **11** 1331

[21] Oh K S, Park S H and Jeong Y K 2004 *Key Eng. Mater.* **264–268** 2111

[22] Zyman Z, Rokhmistrov D, Ivanov I and Epple M 2006 *Materialwiss. Werkst.* **37** 530

[23] Iqbal N, Kadir M R A and Malek N A Z N 2012 *Mater. Lett.* **89** 118

[24] Ciobanu C S, Iconaru S L, Chifiriuc M C, Costescu A, Coustumer P L and Predoi D 2013 *Biomed. Res. Int.* **2013** doi: 10.1155/2013/916218

[25] Panacek A, Kvıtek L, Prucek R, Kolar M, Vecerova R, Pizurova N, Sharma V K, Tatjana N and Zboril Z 2006 *J. Phys. Chem. B* **110** 16248

[26] Raimondi F, Scherer G G, Kotz R and Wokaun A 2005 *Angew. Chem. Int. Edit.* **44** 2190

[27] Morones J R, Elechiguerra J L, Camacho A, Holt K, Kouri J B, Ramırez J T and Yacaman M J 2005 *Nanotechnology* **16** 2346

[28] Pal S, Tak Y K and Song J M 2007 *Appl. Environ. Microb.* **73** 1712

[29] Mulvaney P 1996 *Langmuir* **12** 788

[30] Kreibig U and Vollmer M 1995 *Optical properties of metal clusters* (Berlin, Germany: Springer)

[31] Yang L, Ning X, Xiao Q and Zhou K H 2007 *J. Biomed. Mater. Res. Part B: Appl. Biomater.* **81B** 50

[32] Feng Q L, Kim T N, Wu J, Park E S, Kim J O, Lim D Y and Cui F Z 1998 *Thin Solid Films* **335** 214

[33] Bai X, More K, Rouleau C M and Rabiei A 2010 *Acta Biomater.* **6** 2264

[34] Vijayalakshmi U and Rajeswari S 2012 *J. Sol–Gel Technol.* **63** 45

[35] Jovanovic J, Adnadjevic B, Kicanovic M and Uskokovic D 2004 *Colloids Surf. B: Biointerfaces* **39** 181

[36] Nath S, Kalmodia S and Basu B 2010 *J. Mater. Sci.: Mater. Med.* **21** 1273

[37] Smith D J, Petfordlong A K, Wallenberg L R and Bovin J O 1986 *Science* **233** 872

[38] Liu H B *et al* 2001 *Surf. Sci.* **491** 88

[39] Yacaman M J, Asencio J, Liu H B and Gardea J J 2001 *J. Vac. Sci. Technol. B* **19** 1091

[40] Buckley J J, Lee A F, Olivi L and Wilson K 2010 *J. Mater. Chem.* **20** 8056

[41] Yi Z, Ye J, Kikugawa N, Kako T, Ouyang S, Stuart-Williams H *et al* 2010 *Nat. Mater.* **9** 559

[42] Iqbal N, Kadir M R A and Malek N A N N 2013 *Mater. Res. Bull.* **48** 3172

[43] Akhavan A, Sheikh N, Khoylou F, Naimian F and Ataeivarjovi E 2014 *Radiat. Phys. Chem.* **98** 46

[44] Ciobanu C S, Iconaru S L, Coustumer P L, Constantin L V and Predoi D 2012 *Nanoscale Res. Lett.* **7** 324

[45] Sygnatowicz M, Keyshar K and Tiwari A 2010 *J. Mater.* **62** 65

[46] Mocanu A, Furtosa G, Rapuntean S, Horovitz O, Flore C, Garboa C *et al* 2014 *Appl. Surf. Sci.* **298** 225

[47] Singh R P and Batra U 2014 *J. Chem. Pharm. Res.* **6** 469

[48] Castanon G A M, Martınez N N, Gutierrez F M, Mendoza J R M and Ruiz F 2008 *J. Nanopart. Res.* **10** 1343

[49] Li W R, Xie X B, Shi Q S, Duan S S, Ouyang Y S and Chen Y B 2011 *Biometals* **24** 135

[50] Marini M, De Niederhausern, Iseppi R, Bondi M, Sabia C, Toselli M and Pilati F 2007 *Biomacromolecules* **8** 1246

[51] Stanic V, Janackovic D, Dimitrijevic S, Tanaskovic S B and Mitric M 2011 *Appl. Surf. Sci.* **257** 4510

[52] Lim P N, Teo E Y, Ho B, Tay B Y and Thian E S 2013 *J. Biomed. Mater. Res.* **101A** 2456